FEATURE ARTICLE

Product State Resolved Dynamics of Elementary Reactions

Mark Brouard,* Patrick O'Keeffe, and Claire Vallance

The Physical and Theoretical Chemistry Laboratory, The University of Oxford, South Parks Road, Oxford, OX1 3QZ, U.K.

Received: August 29, 2001; In Final Form: December 17, 2001

We describe how the photon-initiated reaction technique has been used to provide dynamical information about elementary gas-phase bimolecular reactions at the product quantum state-resolved level. The primary focus is on the product angular scattering and rotational angular momentum polarization information that can be obtained from bulb experiments. We illustrate how particular insight into the reaction mechanism is provided by comparisons with the results of model calculations and with ab initio theoretical predictions obtained by others in the field. We show how the experimental measurements have helped provide a critical assessment of the ability of current theory to predict the outcome of simple chemical reactions. The bimolecular systems discussed include the reaction of $O(^1D)$ with H_2 and the H atom reactions with H_2O and N_2O. Measurement of angular momentum orientation is also illustrated by reference to the photodissociation on NO_2. Future developments of the photon-initiated reaction technique are also discussed.

1. Introduction

Elucidating the dynamics of elementary chemical reactions from first principles is a goal which lies at the very heart of physical chemistry;[1] yet, the inherent complexity of molecular collisions necessitates the use of approximations to render them theoretically tractable. The most familiar simplification is the Born−Oppenheimer approximation, which allows the dynamical description of reactions in terms of the motion of nuclei over isolated potential energy surfaces (PESs). However, for all but the very simplest processes, one is generally forced to approximate the dynamics still further by using reduced dimensionality quantum mechanical (QM) treatments[2−4] or quasiclassical trajectory (QCT) methods.[4,5]

Whatever the level of approximation, the methods employed must be validated, and the ultimate test for theory lies in the comparison with experiment. The main focus of our research over the past few years has been helping to provide such experimental data using laser pump−probe techniques.

An important element for us has been the study of reactive systems at the forefront of what is theoretically possible, for which the interplay between experiment and theory can be most informative. Several key areas of theoretical development are illustrated by the choice of reactions we have highlighted in this paper. These include reactions proceeding via deep potential energy wells, such as the insertion reaction $O(^1D) + H_2 \rightarrow OH + H$, that have only become amenable to rigorous quantum mechanical study in the past few years.[6] The development of QM treatments of reactions involving more than three atoms is another major area of theoretical research, which is typified by studies of the benchmark $H + H_2O$ reaction.[7] Here the theoretical challenge has been not only to solve the nuclear dynamics problem quantum mechanically[4,8] but, perhaps more fundamentally, to develop efficient methods for calculating accurate *global* potential energy surfaces for larger chemical systems.[9] A third area has been understanding the role of excited electronic states and, in particular, nonadiabatic effects in chemical reactions,[10,11] an issue which is again pertinent to the $O(^1D) + H_2$ reaction.[12]

There are now several beautiful examples in the literature which demonstrate the high level of agreement between experiment and theory that can be achieved for relatively simple chemical processes. The direct three-atom reactions $H + H_2/D_2$[13] and $F + H_2$[14] provide well-known but nonetheless impressive examples. However, as the chemical complexity increases, one is forced to use simpler models to help interpret experimental data. Although such models might be very approximate, they can still provide insight about the reaction mechanism, as we hope to illustrate by reference to the H atom reactions with H_2O and N_2O.

The paper is planned as follows. Section 2 describes the types of experimental measurements which have been made. There have been several reviews in recent years of the pump−probe technique that we employ,[15−20] so we have strived to keep this section as brief as possible. In the subsequent sections, we illustrate measurements of the quantum state populations of the nascent state-resolved reaction products (section 3), their angular scattering and kinetic energy release distributions (section 4), and finally their rotational angular momentum alignment (section 5) and orientation (section 6). Throughout, we compare our data with the results of high quality dynamical calculations, performed by others in the field. We close with a brief look forward to some future experiments (section 7).

2. Methodology

We employ a variant of flash photolysis,[21] termed the photon-initiated reaction technique.[22−25] The process is depicted

* To whom correspondence should be addressed. E-mail: mark.brouard@chem.ox.ac.uk.

10.1021/jp015530b CCC: $22.00
Published on Web 03/05/2002

SCHEME 1

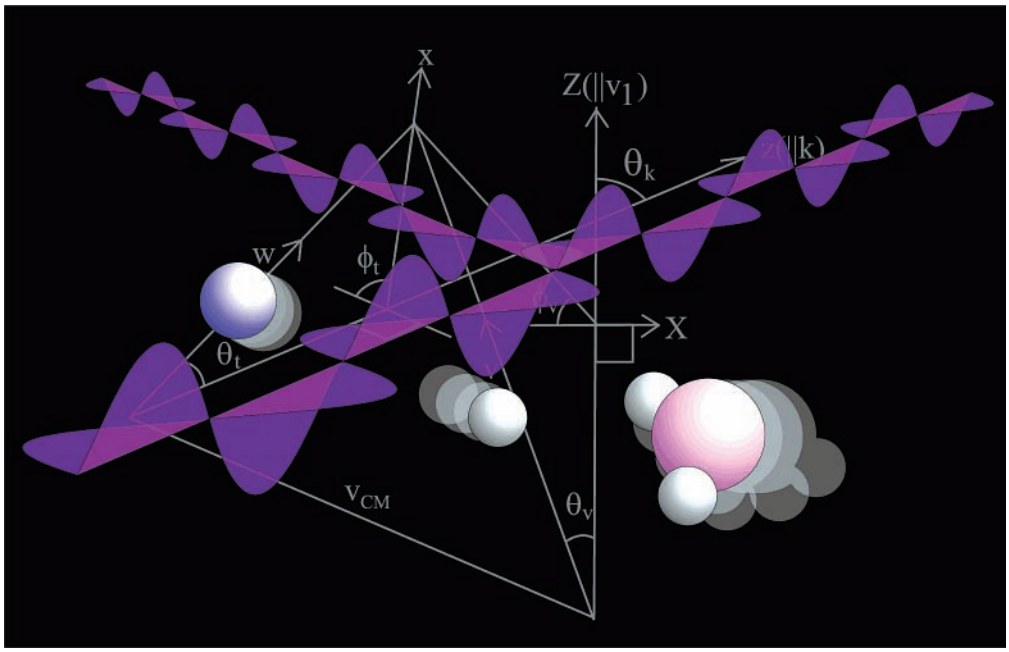

schematically in Scheme 1 and may be characterized by the reaction sequence

$$AX + h\nu \rightarrow A + X \quad (1)$$

$$A + BCD \rightarrow AB(v', j') + CD \quad (2)$$

where we have specialized step 2 to a four-atom reaction. Translationally excited atoms, A, are produced by pulsed, polarized laser photolysis of a suitable precursor molecule (AX), which is held in a low pressure, room-temperature gaseous mixture along with an equal quantity of target BCD molecules. After a short time-delay, sufficient to allow some reaction via step 2 to take place, the AB(v', j') products are probed by laser induced fluorescence (LIF) using the polarized radiation from a second tunable laser. Experiments of this type have been used previously to provide information about product quantum state populations and reaction cross-sections,[26] but our particular emphasis has been obtaining product quantum state-resolved vectorial information about elementary reactions.

As an example, the laboratory (LAB) frame three-dimensional velocity distribution of the nascent quantum state resolved products can be derived from a series of one-dimensional projections of that distribution. These projections are obtained by recording a series of Doppler broadened line shapes of individual rovibronic LIF transitions at high resolution (so-called Doppler-resolved profiles) in different pump−probe laser geometries. Fortunately, the LAB frame angular distribution of the reaction products, AB(v', j'), has the same functional form as that of the photofragments, A, generated in step 1,[27,28] and therefore, only two such projections (Doppler profiles) are required to characterize fully the LAB distribution. As illustrated below, the measurements allow determination of the dynamically interesting center-of-mass (CM) angular scattering distribution of the state-resolved AB(v', j') products, which is proportional to the differential cross-section. This quantity characterizes the direction of the product relative velocity $\mathbf{k}'$ with respect to that of the reactants $\mathbf{k}$. From the same measurements, information about the kinetic energy release into the channel leading to AB(v', j') can also be extracted. Therefore, by applying conservation of energy, it is possible to infer the internal energy disposal in the CD cofragment that partners the detected state-resolved AB(v', j') product.

In practice, the raw Doppler profiles are related to the CM frame velocity distribution through a complicated frame transformation,[22−25] and it is not possible to invert the experimental data directly. Instead, a fitting procedure is employed, which we illustrate in Figure 1.[29,30] The method first involves generating linear combinations of raw experimental Doppler profiles recorded in (at least) two laser pump−probe geometries. These combinations, which are called composite Doppler profiles, depend separately on the LAB speed and translation anisotropy terms of the full LAB velocity distribution. The two composite profiles (shown at the bottom left of Figure 1) are then fitted with a linear combination of basis functions. The triple scattering angle-recoil energy differential cross section can be expressed in terms of a series of Legendre polynomials

$$\frac{2\pi\ \mathrm{d}^3\sigma}{\sigma\ \mathrm{d}\omega_t \mathrm{d}f_t} = P(f_t, \cos\theta_t) = \frac{1}{4}\sum_{n,m} a_{nm} P_n(\cos\theta_t) P_m(f_t') \quad (3)$$

where θ_t is the CM scattering angle, $f_t' = (2f_t - 1)$, and f_t is the fraction of the available energy released into translation. The basis functions (shown on the upper left of Figure 1) represent the contribution of each Legendre moment to the overall composite profile and are calculated by convoluting the different products of Legendre polynomials $P_n(\cos\theta_t) \times P_m(f_t')$ (see the upper right panels of Figure 1) with the precursor and target thermal velocity distributions[22,23,32−34] and by transforming from the CM to the LAB system. The relative weight of each individual basis function is thus given by the coefficients a_{nm} of the expansion given in eq 3, which are determined by simultaneously fitting the two composite profiles described above[29,31] (see the bottom right panel of Figure 1). The number of expansion terms employed in the fits, and hence in the reconstruction of the CM distribution via eq 3, depends on a number of factors including the kinematics and energetics of the particular reaction studied, but as a rule of thumb, converged fits to experimental data are usually obtained with $n \sim m \leq 5$. The number of Legendre moments employed effectively determines the angular and energy release resolution of the experi-

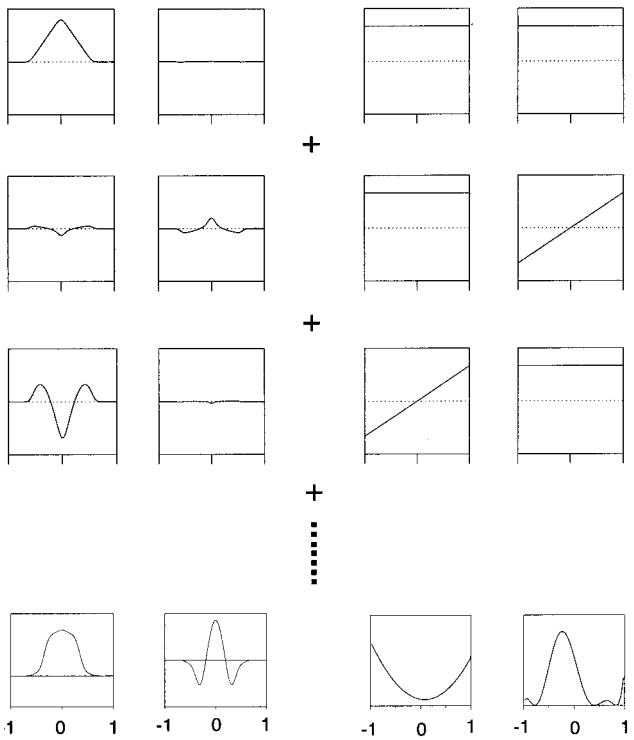

Figure 1. Upper three rows illustrate the basis functions employed in the fitting procedure described in section 2. The four columns (from left to right) are the basis functions for the OH LAB speed and LAB translational anisotropy composite profiles and the relevant Legendre polynomial functions of the CM angular scattering and kinetic energy release distributions employed in their generation. The bottom row shows the linear combination of basis functions used to fit the experimental data (left two panels) and the recovered CM angular scattering and kinetic energy release distributions of interest (right two panels).

ments. The CM angular distribution $P(\cos\theta_t)$ (equivalent to the normalized differential cross-section $(2\pi/\sigma)$ $(d\sigma/d\omega_t)$) is obtained by integrating eq 3 over f_t, whereas the distribution over the fractional kinetic energy release $P(f_t)$ is obtained by integration over scattering angle.

The LIF intensity is also sensitive to anisotropy in the angular distribution of the product rotational angular momentum vector, $\mathbf{j}'$.[27,34,35−37] The LIF absorption transition probability depends on the alignment of the electronic transition moment of the fragment, μ_{AB}, with respect to the electric vector of the probe radiation. In the high j' limit, the transition moment lies either parallel (for Q↑ transitions) or perpendicular (for P↑ or R↑ transitions) to $\mathbf{j}'$. Therefore, if the nascent reaction products are rotationally polarized in the laboratory (LAB; i.e., if $\mathbf{j}'$ lies in a preferred direction, see section 5), the LIF intensity will depend on the degree of this polarization.[27] Detailed measurements of LIF intensity and Doppler-resolved line shape as a function of the pump and probe laser polarizations allow moments of the rotational angular momentum distribution of the reaction products and its dependence on CM scattering angle to be characterized:[23,35−37] such studies provide an insight into the angular distribution of $\mathbf{j}'$ with respect to the vectors $\mathbf{k}$ and $\mathbf{k}'$, which define the reference scattering plane.

In the semiclassical limit, the CM polarization distribution of interest can be written[23,25]

$$P(\cos\theta_t,\omega_{j'}) = \frac{1}{4\pi}\sum_{kq}[k]\frac{2\pi}{\sigma}\frac{d\sigma_{kq}}{d\omega_t}C^*_{kq}(\omega_{j'}) \qquad (4)$$

where $[k] = 2k + 1$, $C_{kq}(\cdot\ \cdot\ \cdot)$ are the modified spherical harmonics, and the solid angles $\omega_{j'}$ are measured with respect to the CM $\mathbf{k}-\mathbf{k}'$ scattering plane. A rigorous QM expression has been provided by Miranda and Clary,[38] and the relationship between the QM and classical polarization parameters in the correspondence limit has been discussed by Aoiz and Miranda and co-workers,[39] which also presents a detailed study of polarization effects in the $H + D_2$ reaction. The CM parameters $(2\pi/\sigma)$ $(d\sigma_{kq}/d\omega_t)$ are known as polarization dependent differential cross-sections (PDDCSs)[25] and characterize the scattering angle dependence of the rotational polarization. The first expansion coefficient, with $k,q = 0$, is simply the angular scattering distribution $P(\cos\theta_t)$ discussed above, whereas that for $k = 2$ and $q = 0$, for example, describes the variation in the rotational angular momentum alignment with scattering angle (see further below). Low order moments of the full CM distribution, typically with $k \leq 2$ or 3, can be extracted from the dependence of the Doppler profiles on laser polarization and rotational branch using similar procedures to those employed to determine the differential cross-section[40] (see above). If linearly polarized photolysis *and* probe light are used, the index k is restricted to even values, with $k \leq 4$.[35] Terms with odd k indices can only be determined using circularly polarized probe radiation[36] (see further discussion in sections 5 and 6). As will also be shown in sections 5 and 6, once the PDDCSs are known, eq 3 can be used to recover (or partially recover) the rotational angular momentum polarization distribution as a function of CM scattering angle.

Finally, integration of the PDDCSs over scattering angle yields the (scattering angle averaged) polarization parameters a^k_q.[23,25,39] The term most readily determined is the CM rotational alignment parameter a^2_0, because it can be obtained directly from measurements of the variation of *integrated* LIF intensity with laser polarization and probe transition (see section 5). In the high j' limit, this CM frame alignment can be interpreted as the second Legendre moment $a^2_0 = \langle P_2(\hat{\mathbf{k}}\cdot\hat{\mathbf{j}}')\rangle$ of the $\mathbf{k}-\mathbf{j}'$ distribution.[27,34,35,38,39] It ranges in value from -0.5 to $+1$, with the two limits corresponding to $\mathbf{j}'$ perpendicular and parallel to $\mathbf{k}$, respectively.

3. Populations

3.1. The $H + H_2O \rightarrow OH + H_2$ Reaction. The H atom reaction with H_2O is isoelectronic with the $H + HF$ abstraction reaction, i.e., the reverse of $F + H_2$: it is a direct process with a barrier of ~0.9 eV in the forward direction and an endothermicity of ~0.6 eV.[4] OH rovibrational populations have been determined previously for this reaction, principally by the group of Wolfrum.[20,41] The population distributions have been compared with the results of a number of QCT studies[42−45] using a variety of PESs.[44,46−48] The fact that the distributions are rather cold suggests that the OH bond preserved during the reaction acts as a spectator; this picture is reinforced by the bond selective experiments of Crim and co-workers,[49] who studied the H atom reactions with vibrationally excited water molecules (see ref 20). They showed that the conserved OH bond in the HOH target molecule behaves vibrationally adiabatically during reaction[49] (see further discussion in section 4.1.).

At low collision energies, the $OH(v' = 0)$ rotational excitation arising from reaction with ground-state water molecules (together with more subtle features such as the OH Λ-doublet population propensities[50]) can be modeled using a modified Franck−Condon model[51] originally devised for the photodissociation of $H_2O(\tilde{A})$.[52] Similar Franck−Condon models have previously been proposed by Clary and co-workers.[53,54] The

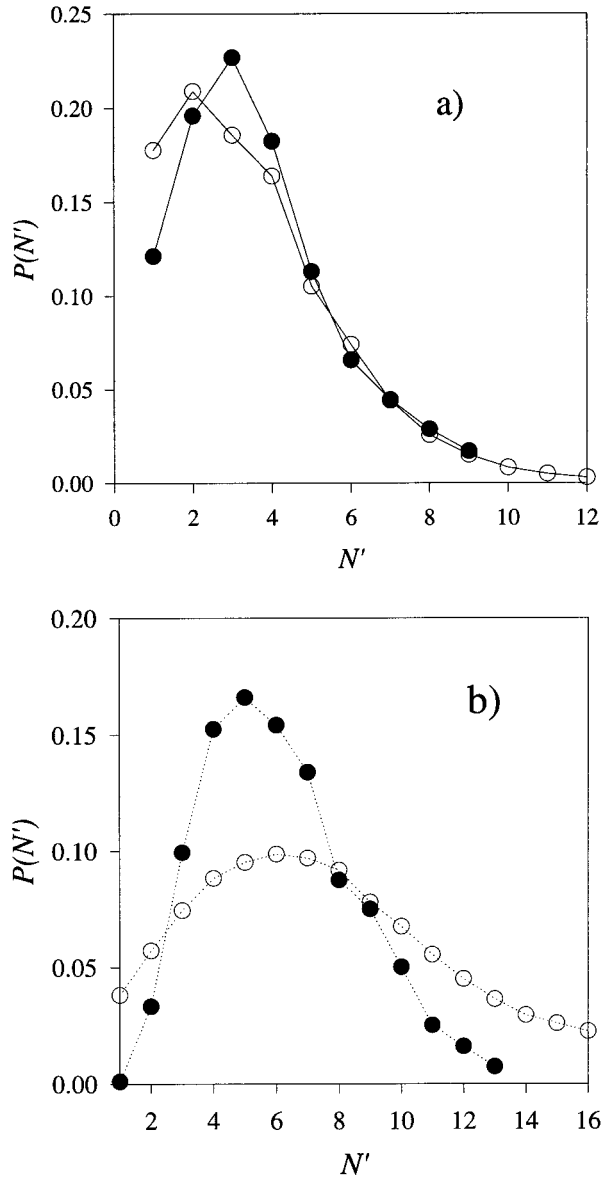

Figure 2. (a) Product rotational distributions for $H + H_2O$ at a collision energy of 1.4 eV. Full circles (●), the OH($v' = 0$, N') rotational distribution determined experimentally, averaged over lambda-doublet and spin−orbit state; open circles (○), results of the Franck−Condon model described in section 3. (b) Comparison between the experimental rotational distribution (●) for the $H + H_2O$ reaction at 2.5 eV with the probabilities derived using QCT methods[43] and the OC PES.[47] Note that in this figure we have equated the *open shell* N' values used experimentally (which represent the total OH angular momentum apart from electron spin) with $j' + 1$, where j' is the rotational angular momentum used in the *closed shell* calculations.

essential feature of these models is that product rotation is assumed to arise solely from rotational and bending motions in the reactant H_2O molecule, with no torques being exerted on the OH moiety during reaction. Experimental population data for the H atom reaction with H_2O at a collision energy of 1.4 eV are compared with the model calculations in Figure 2a.[55] The data reveal that the majority of the OH rotation at 1.4 eV comes from rotational and zero-point bending motion in the parent water molecule and confirms that OH indeed behaves as a spectator. (It may come as no surprise that OH rotational angular momentum alignment at this collision energy is very small.[56] In the spectator limit, the direction of $\mathbf{j}'$ would be isotropic, reflecting the isotropic angular momentum distribution in the H_2O reactant.)

As the collision energy is raised, a small increase in OH product rotational excitation is observed, consistent with some momentum transfer from the incoming H atom to the OH moiety of the target molecule.[41,56] The rotational distribution determined at a collision energy of 2.5 eV is shown in Figure 2b,[56] in which the data are compared with QCT dynamical calculations[57] performed on the recently developed PES by Ochoa and Clary (known as the OC PES).[47] The calculations tend to overestimate the OH rotational (and vibrational) excitation (i.e., in the QCT calculations, OH appears to behave less as a spectator than observed experimentally). More recent QCT theoretical studies yield lower levels of OH internal excitation[45,57] and reveal that, despite the apparent spectator-type behavior of the unreactive OH(OD) bond, the predicted OH(OD) rotational distributions are rather sensitive to the details of the PES employed.

3.2. The $O(^1D) + H_2 \rightarrow OH + H$ Reaction. The theoretical importance of this reaction has already been touched on in section 1. The electronic degeneracy of the oxygen atom leads to the possibility of reaction over one or more of five different PESs.[12,58] All of these surfaces are Coriolis coupled in the entrance channel, but only the lowest three are believed to play an important role in the reaction dynamics at collision energies $E_t \sim 0.1$ eV.[58] The deep well on the $1^1A'$ ground-state surface corresponds to bound H_2O; on this surface, reaction proceeds predominantly via an insertion mechanism, with the transient H_2O intermediate dissociating to give a near-statistical distribution of energy over accessible product quantum states.[6,59] The situation is very different for reaction over the first excited ($1^1A''$) surface.[12,60] A 0.1 eV barrier is present in the entrance channel, and reaction occurs via an abstraction mechanism.[12,60,61] There is a strong population inversion in the product vibrational state distribution, with OH formed almost exclusively in the $v' = 3$ and′ 4 vibrational levels.[12,60] The second excited state ($2^1A'$) surface also has a barrier to reaction but correlates with electronically excited OH products. Reaction over this surface involves nonadiabatic coupling through a conical intersection with the ground state and results in a similar broad-ranging product state distribution to that obtained for reaction solely over the ground-state surface.[58,61,62]

For the products of reaction over excited surfaces to be observable experimentally, they must make up a significant fraction of the product yield in the particular product quantum state(s) detected. This requirement makes it unlikely that experimental evidence will be readily found for reaction over the $2^1A'$ surface at collision energies around 0.1 eV but is satisfied for reaction over the $1^1A''$ surface, because even though the fraction of reaction proceeding over this surface is small product flux is concentrated in a small range of quantum states. Participation of the $1^1A''$ surface had been suggested previously on the basis of crossed beam measurements of the collision energy dependence of the total angular differential cross section[63] and from hydrogen atom LIF measurements of the excitation function,[64] but the interpretation of these experiments was complicated by the lack of product quantum state resolution. We have shown that detailed comparison of OH product rotational population distributions (and rotational alignment parameters, see section 5) with the results of rigorous QCT and QM scattering calculations provides strong evidence for involvement of the $1^1A''$ surface at energies above 0.1 eV.[65] The measurements highlight the benefits of (and necessity for) product quantum state resolution: the beautiful H-atom Rydberg tagging time-of-flight experiments of Yang and co-workers,[66] which now provide close to product quantum state resolution, reinforce the interpretation of the LIF measurements[65] that the

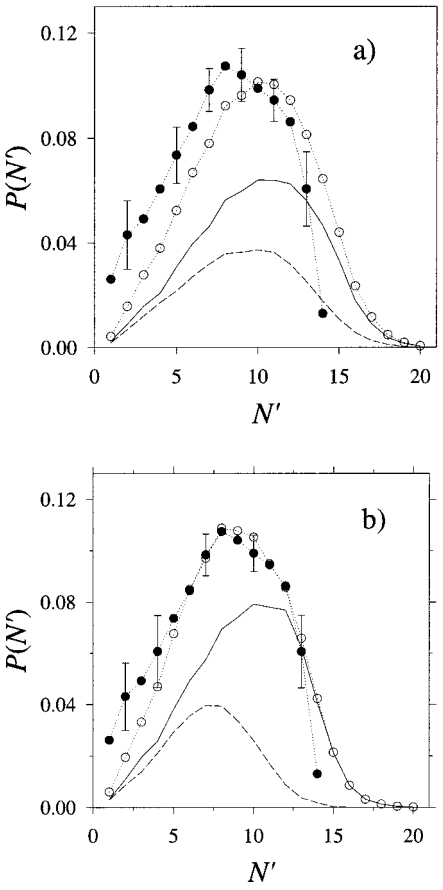

Figure 3. (a) Comparison between the experimental rotational populations for the OH($v' = 4$) products of the O(^{1}D) + H_2 reaction (solid circles with error bars) with those derived from QCT calculations[67] including reaction on both the $1^1A'$ and $1^1A''$ DK PESs. (b) The same as that for part a except the comparison is with the populations derived from QM calculations including reaction on both the $1^1A'$ and $1^1A''$ DK PESs. In both figures, the continuous solid lines represent the contribution from the A′ PES, whereas those from the A″ PES are shown as dashed lines. Adapted from ref 65.

$1^1A''$ surface participates in the reaction at collision energies above 0.1 eV.

In our work, the experimental rotational population distributions have been compared with the predictions of scattering calculations, both with and without the inclusion of contributions from reaction over the $1^1A''$ surface.[65] The calculations employed the Dobbyn and Knowles (DK) versions of the ground and excited-state PESs.[61] At first glance, both QCT and QM scattering calculations reproduce the measured rotational distributions reasonably well, but on closer examination, several differences become apparent. These are illustrated for the $v' = 4$ rotational distribution (Figure 3). Reaction over the ground-state surface produces a hotter rotational distribution than reaction over the excited surface, so that inclusion of the excited-state surface in the calculations has the effect of shifting the overall distribution to lower rotational quantum number. For both the QCT and the QM scattering calculations, this improves agreement with experiment (the separate contributions to the populations from reaction over each PES are also shown in Figure 3). Although the QCT results reproduce the measured $v' = 4$ rotational distribution reasonably closely, they are shifted to higher rotational quantum number and span a wider range of rotational quantum states than found experimentally (see Figure 3a). In contrast, the QM scattering results are in near-perfect agreement with experiment[65] once contributions from

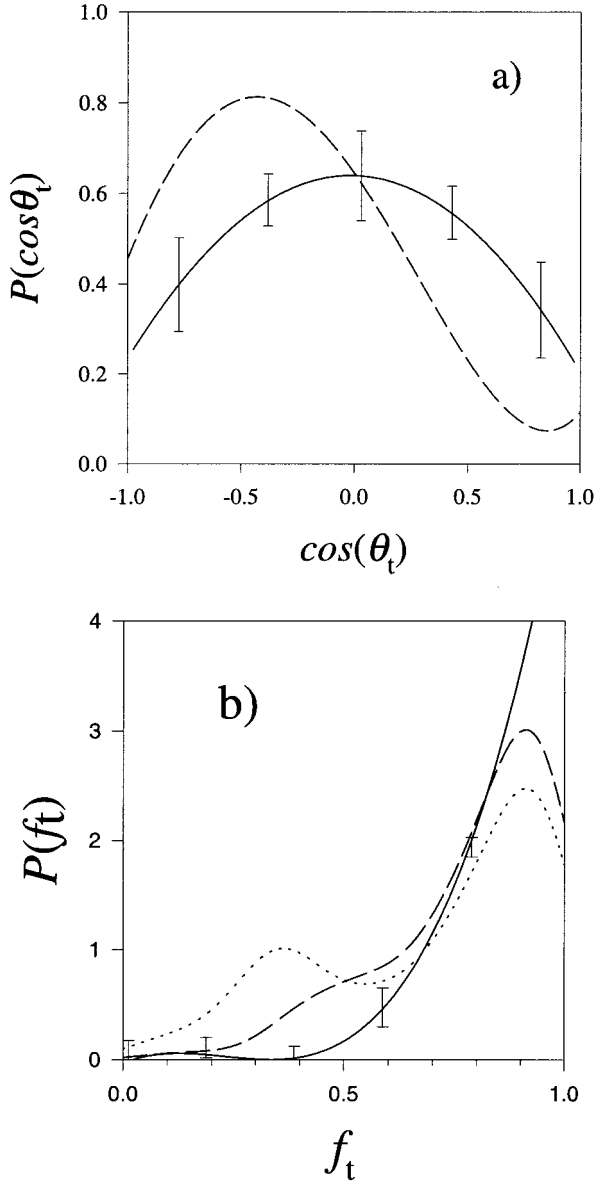

Figure 4. (a) Comparison between the experimental angular scattering distribution (smooth line with error bars) for the H + H_2O reaction born in OH($^2\Pi_{1/2}$, $v' = 0$, $N' = 1$), and that derived from the QCT calculations of Aoiz and Castillo and co-workers[43] using the OC PES.[47] (b) Comparison between the experimental kinetic energy release distribution (smooth line with error bars) for the H + H_2O reaction generating OH($v' = 0$, $N' = 1$) products at a mean collision energy of 1.4 eV, and those simulated using H_2 rovibrational populations determined from QCT calculations[43] on the OC PES.[47] The simulations are shown with (dotted) and without (dashed) inclusion of the contributions from $H_2(v'' = 1)$. In both parts a and b, the QCT data are specific to channels yielding OH($v' = 0$, $j' \leq 2$). Adapted from ref 55.

reactive scattering over the excited $1^1A''$ state are included (see Figure 3b). Further evidence for the involvement of the excited-state surface will be presented in section 5.

4. CM Angular Distributions

4.1. The H + H_2O → OH + H_2 Reaction. The angular scattering distribution, $P(\cos\theta_t)$, for the A' Λ-doublet level of OH($^2\Pi_{1/2}$, $v' = 0$, $N' = 1$) produced from the title reaction at a collision energy of 1.4 eV is shown in Figure 4a,[31,55] where it is compared with the results of Castillo and co-workers[42] using the OC PESs.[47] The latter calculations are just one of a number

of recent QCT studies which have been performed[44,45,48] using different PESs. Experimentally, the angular scattering distributions are found to be rather insensitive to OH rotational state (consistent with the OH spectator type behavior discussed in section 3.1.) and to OH Λ-doublet level.[55] The fact that the angular distribution is very broad is at first-sight surprising, given that strong rebound dynamics are observed for the reverse reaction at low collision energies.[68,69] However, the broad angular scattering is qualitatively in agreement with QCT predictions using the most recent PESs[42,44,45,48] (see for example the data shown in Figure 4a). The results suggest that the H-atom reaction possesses a wide "cone of acceptance" at the elevated collision energies employed in the hot-atom experiments.[31] A much more dramatic opening in the cone of acceptance occurs upon vibrational excitation of the water target molecule[49,70] (see section 3.1.). Guided by the experiments of Crim and co-workers,[49] Smith and co-workers[71] have recently quantified the enhancements in reaction rate which occur when water is excited into a series of vibrational overtone states. The enhancements observed when OH stretching modes are excited are many orders of magnitude greater than those obtained when similar amounts of energy are placed into translation (as in the present experiments), a result which is consistent with the reaction having a late barrier.[71]

The reaction of H atoms with D_2O at a collision energy of 1.4 eV generates predominantly backward scattered products. As the collision energy is raised, the scattering moves toward the forward hemisphere.[55,56] The behavior is qualitatively reproduced by QCT theoretical predictions using the recent OC[57] and the WSLFH[45] PESs. The deuterated reaction appears to show a stronger propensity for backward scattering than its protonated cousin; this is perhaps not unexpected because the reaction cross-section for $H + D_2O$ is significantly smaller than that for $H + H_2O$.[7,26,45] Although tunneling (in the lighter system) may play a role, the fact that the general trends appear to be reasonably well accounted for using QCT methods suggests that the main difference between the two isotopic reactions is the difference in reactant zero-point energy, which in the deuterated case this leads to a higher effective barrier to reaction (and trajectories which more closely follow the minimum energy pathway). Kinematic factors, analogous to those which determine the relative cross-sections of the $H + D_2$ and $D + H_2$ abstraction reactions,[72] may also play an important role.[57]

As discussed in section 2, the Doppler resolved LIF profiles also contain information about the OH state-resolved kinetic energy releases. Figure 4b shows the distribution of the fractional kinetic energy release $P(f_t)$, again for the $OH(^2\Pi_{1/2}, v' = 0, N' = 1, A')$ products of the $H + H_2O$ reaction at 1.4 eV. At this collision energy, the $OH + H_2$ products are born with high kinetic energy, and hence, from energy conservation, the H_2 coproducts must be produced rovibrationally cold. The data are compared once more with the QCT results of Castillo et al.[43] using the OC PES:[47] the agreement between experiment and theory is qualitative only, with the calculations overestimating the H_2 internal excitation. Similar calculations by Schatz and co-workers[45] using the recent WSLFH PES[48] seem to yield even greater HD excitation at 1.4 eV compared with the OC PES results, even though the WSLFH PES provides better agreement with experiment than the OC PES for the OH energy disposal (see above). The experimental data should also be compared with the high collision energy HD REMPI study of the $H + D_2O$ reaction by Zare and co-workers,[70] which showed significantly higher $HD(v'', j'')$ rovibrational excitation than we have observed indirectly at 1.4 eV.[55] However, our own work on the $H + D_2O$ reaction at 2.5 eV, an energy which approaches those sampled in the experiments of Zare and co-workers,[70] indicates very similar HD excitation to that observed more directly in the REMPI study,[70] suggesting that there is a real (and significant) change in HD energy disposal with increasing collision energy. Although QCT[44,45,48,57] and QM ($J = 0$)[73] calculations indicate an increase in H_2/HD internal excitation with increasing collision energy, a quantitative explanation must await more detailed calculations. In particular, converged QM calculations are required to establish whether discrepancies between theory and experiment are due to inaccuracies in the PESs employed and/or arise from inadequacies in the QCT method, particularly the treatment of zero-point energy constraints.

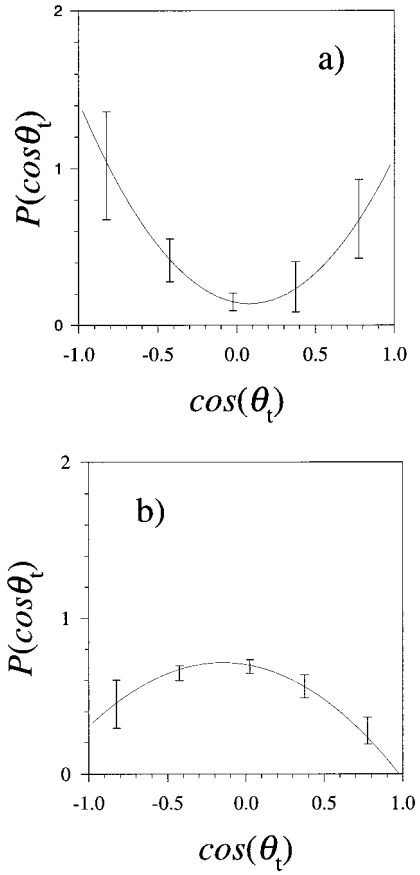

Figure 5. CM angular distributions for $H + N_2O$ reaction generating $OH(^2\Pi_{3/2}; A'')$ products in $v' = 0$, $N' = 5$ (a) and 14 (b). The error bars represent 2σ uncertainties. The data are taken from refs 29 and 74.

4.2. The $H + N_2O \rightarrow OH + N_2$ Reaction. As we have seen, the H atom reaction with H_2O behaves (perhaps reassuringly) like a three-atom reaction: the dynamics appears localized to the H−H−O moiety, with the preserved OH bond behaving like a spectator. The $H + N_2O$ reaction provides a salutary reminder that reactions often do not conform to this simple picture. The angular scattering distributions are found to be exquisitely sensitive to the $OH(v', j')$ quantum state:[29,40,74,75] here the chemistry is not localized to a subset of atoms but intimately involves all four. Example angular scattering data are shown in Figure 5. OH fragments born with low rotational excitation are scattered predominantly in the forward and backward directions, whereas those born in high rotational levels are scattered preferentially in the sideways direction. The distributions show approximate forward−backward symmetry,

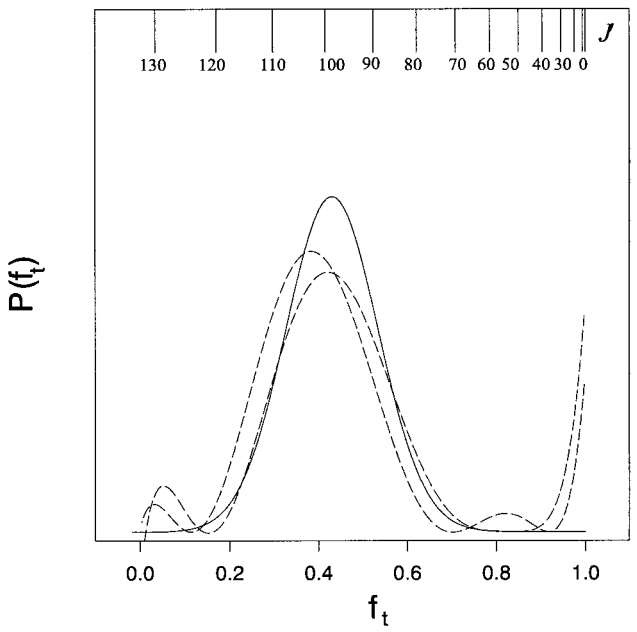

Figure 6. Comparison between the OH($^2\Pi_{3/2}$, $v' = 0$, $N' = 5$) state-resolved kinetic energy release distribution $P(f_t)$ for the reaction of H + N_2O (the two dashed lines, which refer to results for the OH A' and A'' λ -doublet levels)[29] with that obtained in the photodissociation of N_2O via its first absorption band around 205 nm (solid line). The latter distribution has been calculated from the N_2 rotational distribution measured by Kummel et al.[81] The combs at the top of the figure mark the approximate positions of the internal rotational (j') states of the N_2 coproduct of the bimolecular reaction at the mean collision energy of the present experiments. The maximum N_2 vibrational level accessible under these conditions would be $v'_{N_2} \leq 15$.

consistent with the reaction proceeding via a complex.[76] Ab initio and QCT calculations by Schatz and Walch and co-workers[76,77] suggest that a complex, HNNO, may be formed after H atom attack at the terminal N atom of NNO, but the detailed dependence of the angular distributions on OH quantum state is poorly understood. The scattering data are similar to those obtained for the isoelectronic reaction H + CO_2,[78,79] although the angular distributions in that case are more asymmetric, consistent with a rather shorter lifetime for HOCO, relative to the rotational period, compared with HNNO (for a further discussion of the HOCO system see ref 20).

The kinetic energy release distributions $P(f_t)$, which can be determined with relatively high resolution because of the large exothermicity of the reaction, are even more intreguing (see, for example, Figure 6).[29,74,75] They possess a dominant feature at around $f_t \sim 0.5$, which is again attributed to the reaction proceeding via the HNNO complex; the same conclusion had previously been drawn by Wittig and co-workers based on their early Doppler-resolved measurements.[80] In general, the kinetic energy release distributions are less sensitive to the OH quantum state than the angular scattering distributions shown in Figure 5.[29,74,75] However, a small high energy component in the kinetic energy release distribution, just visible in the OH($v' = 0$, $N' = 5$) data shown in Figure 6, grows in magnitude with OH rovibrational excitation and has been assigned to a competing, minor process involving direct H atom attack at the terminal O-atom end of the molecule.[74] QCT calculations by Schatz and co-workers[76,77] suggested (not unreasonably) that the products of the direct channel are born translationally excited but also predicted that the direct mechanism dominates at a collision energy of 1.5 eV, contrary to experimental observation.[74] The study highlights the extreme difficulties in generating reliable global PESs for systems with more than three atoms.

In agreement with the previous work of Wittig and co-workers,[80] the experiments reveal that N_2 is born with remarkably high internal excitation. N_2 products of the reaction have to date not been observed directly, and in an attempt to account for the high N_2 excitation, we have drawn on an analogy between the hot H-atom reaction and the photodissociation dynamics of the "electron poor" species N_2O[81] and HN_3,[82] excited via their first absorption bands. The proposal is that the exit channel (i.e., the NN-X stretching coordinate) for the H atom reaction is similar to those for the photodissociation processes, because similar orbitals are occupied (or partially occupied) in the two systems.[75] As a consequence, the response of the target molecule to the attacking hot H atom should mirror the response of the target (or isoelectronic) molecule to photon excitation to its first excited electronic state. Similar Franck−Condon type arguments have already been introduced in the context of H + H_2O above but have their origins in early studies of the three-atom reactions H + X_2 (X = halogen) by Herschbach and co-workers (see ref 83). In Figure 6 we compare the kinetic energy release distribution observed in the bimolecular reaction with that derived from resonantly enhanced multiphoton ionization (REMPI) measurements of N_2 generated after the 205 nm photodissociation of N_2O by Hanisco and Kummel.[81] These workers demonstrated that N_2 is produced highly rotationally excited, because of the linear-to-bent character of the parent molecular transition. The agreement between the kinetic energy release distributions generated by photodissociation and by bimolecular reaction is remarkable and strongly supports the view that N_2 products generated from the H + N_2O bimolecular reaction are rotationally excited. Note that the N_2 products from the photolysis of HN_3 via the first absorption band are also generated with high levels of rotational excitation:[82,84] as with N_2O, the photolytically generated N_2 fragments have been observed directly by REMPI.[84] In both cases, about 50% of the energy is channeled into N_2 excitation, very similar to that observed in the bimolecular reaction. In a very real sense, the N_2O and HN_3 photodissociation systems can be thought of as "half collisions", in this case the second half of the H + N_2O bimolecular reaction.

There are also strong similarities between the angular scattering distributions generated by the H atom reaction with N_2O (see Figure 5) and those produced by photodissociation of $HN_3(\tilde{A})$, which have been the subject of a detailed study by Gericke and co-workers.[82] In Figure 7, we compare the second moments $\langle P_2(\hat{\mathbf{k}}\cdot\hat{\mathbf{k}}')\rangle$ of the angular distributions determined in the reactive and photodissociation cases.[75] The change in sign of the moments with OH/NH rotational quantum number reflects the change from forward−backward to sideways peaking angular distributions shown in Figure 5 (as mirrored in the photodissociation data[82]). Again, the similarity in the trends for the photodissociation and reactive scattering systems are striking.

5. Angular Momentum Alignment

The rotational angular momentum polarization of reaction products provides information about exit channel bending and torsional torques that are responsible for generating product rotation. Depending on angular momentum conservation constraints and the nature of the angular momentum disposal, the polarization of $\mathbf{j}'$ may also provide information about the distributions of reactant and product orbital angular momenta that are generally unobserved in reactive scattering experiments.[85] Two classes of polarization need to be distinguished, orientation (an odd k moment of the angular momentum distribution, eq 4) and alignment (an even k moment of the

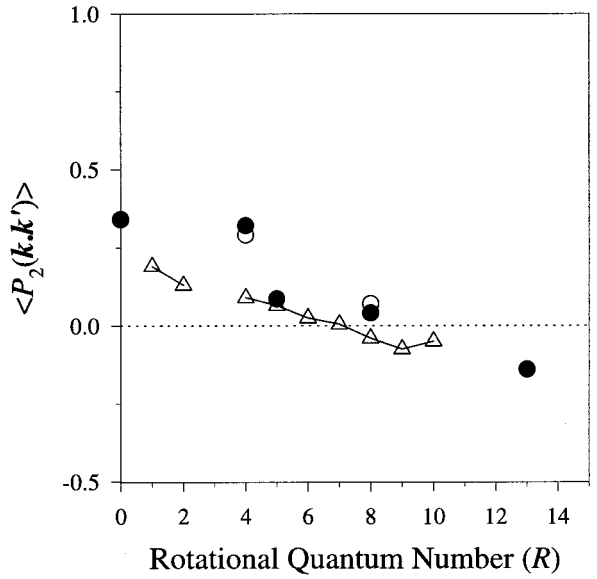

Figure 7. Comparison between the second moments of angular scattering distributions arising from the H + N_2O bimolecular reaction (○ and ●, which refer to OH($^2\Pi_{3/2}$) and OH($^2\Pi_{1/2}$), respectively)[75] with those generated by the photodissociation of HN_3[82] (△). The data in both cases are plotted as a function of *R*, the nuclear rotation quantum number of the OH and NH species. The raw photodissociation data have been transformed as described in ref 75.

distribution). As illustrated in Figure 8 (see further discussion in section 6), alignment measurements reveal whether the product molecule has a preferred axis of rotation, whereas orientation measurements expose the sense or handedness of the rotation. We will deal with these aspects of rotational polarization separately.

5.1. The O(^{1}D) + H_2 → OH + H Reaction. Further evidence for the participation of the excited $1^1A''$ in the title reaction (see section 3.2.) has been provided by the determination of the CM frame rotational alignment parameter a_0^2 (see section 2). For reaction over the ground-state PES, proceeding via an energized HOH insertion complex, one would expect any rotational alignment to be very small, and this is borne out by both QCT and QM scattering calculations.[65] The two sets of calculations are in excellent agreement, both predicting values for a_0^2 of around −0.1 for rotational levels of OH in $v' = 4$ at a collision energy of 0.1 eV.[65] The picture is somewhat different for reaction over the first excited $1^1A''$ surface. In the abstraction reaction, the orbital angular momentum of the approaching O(^{1}D) atom about the H_2 generates a significant torque as the new bond forms. Because this torque is exerted in the scattering plane, the resulting product rotational angular momentum vector **j′** points out of the plane, perpendicular to **k**. QCT and QM scattering calculations carried out for reaction over the $1^1A''$ PES predict alignment parameters of around −0.4, close to the maximum allowed value of −0.5.[65]

Rotational alignments have been measured for OH($v' = 4$; $N' = 3$, 8, 12) and are found to be around −0.2. This is significantly more negative than predicted by calculations carried out purely over the ground-state surface and is consistent with some fraction of reaction proceeding over the $1^1A''$ surface. When the effects of reaction over the excited state surface are included in the calculations, the experimental results are reproduced almost exactly. Figure 9 shows the comparison between the results of QCT calculations, properly averaged over the collision energy distribution of our experiments, and the experimentally measured values of a_0^2.[65]

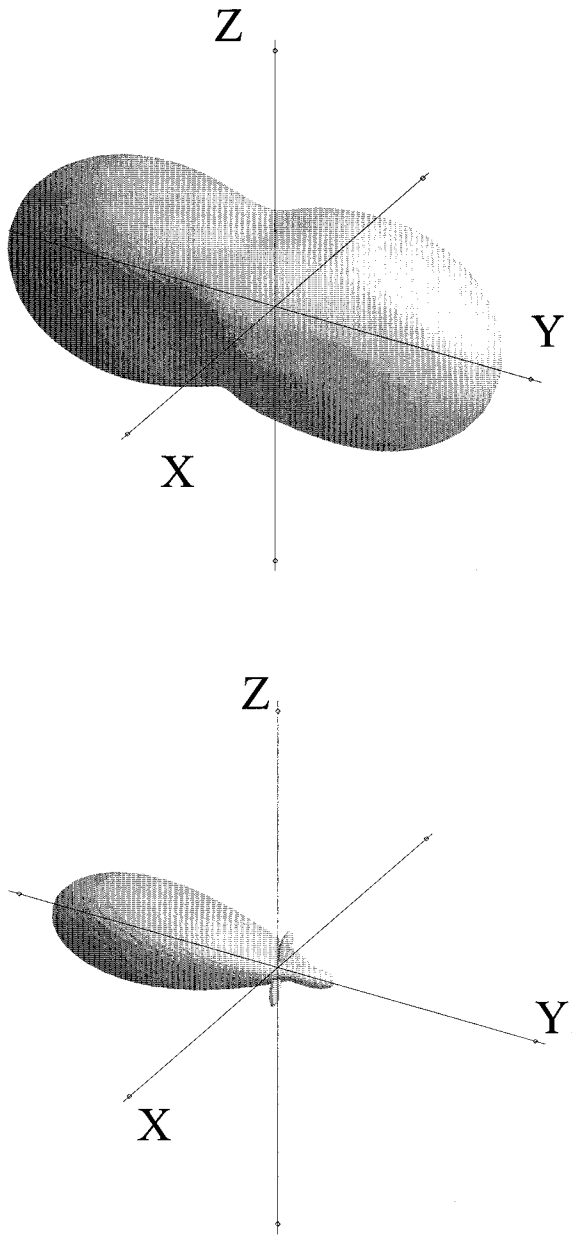

Figure 8. Comparison of the polar plots of the distributions $P(\omega_{j'})$ for OH born in $v' = 4$, $j' = 2$, as predicted for the O(^{1}D) + H_2 reaction by QCT calculations on the K(A′) ground-state PES (upper panel) and K(A″) excited-state PES (lower panel).[86] The collision energy in both cases is 0.1 eV. The figure illustrates that in the case of rotational alignment the rotational motion is preferentially about a particular axis (i.e., about the *z* axis in the upper panel). In the lower panel, the angular momentum vectors preferentially point along the $-y$ axis; that is, they are oriented. The rotational motion is confined in this case to the *zx* plane but also has a well-defined "handedness"; in this example, when viewed from the $+y$ direction, the molecule is rotating in the clockwise direction.

5.2. The H + N_2O → OH + N_2 Reaction. For this reaction, we have been able to resolve the scattering angle dependence of rotational alignment[40] (similar experiments have also been reported for the isoelectronic system H + CO_2[87]). Interestingly, significant alignment effects are only observed in the *A″* Λ-doublet level, with the *A′* level being unpolarized. For the *A″* levels, the Doppler profiles for transitions that originate from the same initial state, but differ only in Δj′, possess different line shapes, an effect which is purely due to OH rotational alignment.[27,40] A full analysis reveals that **j′** preferentially lies parallel to the direction of recoil, **w**, in the CM frame: the results

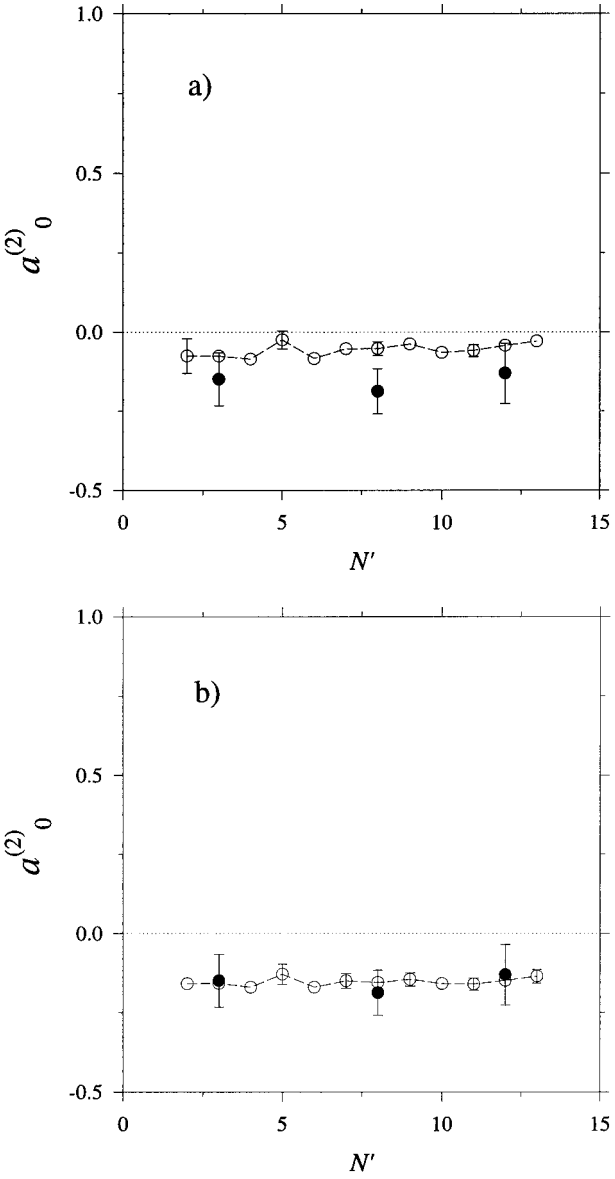

Figure 9. Comparison of the experimental alignment parameters for the OH($v' = 4$) products of the O(^{1}D) + H_2 reaction (solid circles with error bars) with those derived from QCT calculations on the $1^1A'$ DK PES alone (a) and with those including contributions from both the $1^1A'$ and $1^1A''$ DK PES (b). The QCT data have been fully averaged over the experimental collision energy and reagent H_2 rotational distributions. Adapted from ref 65.

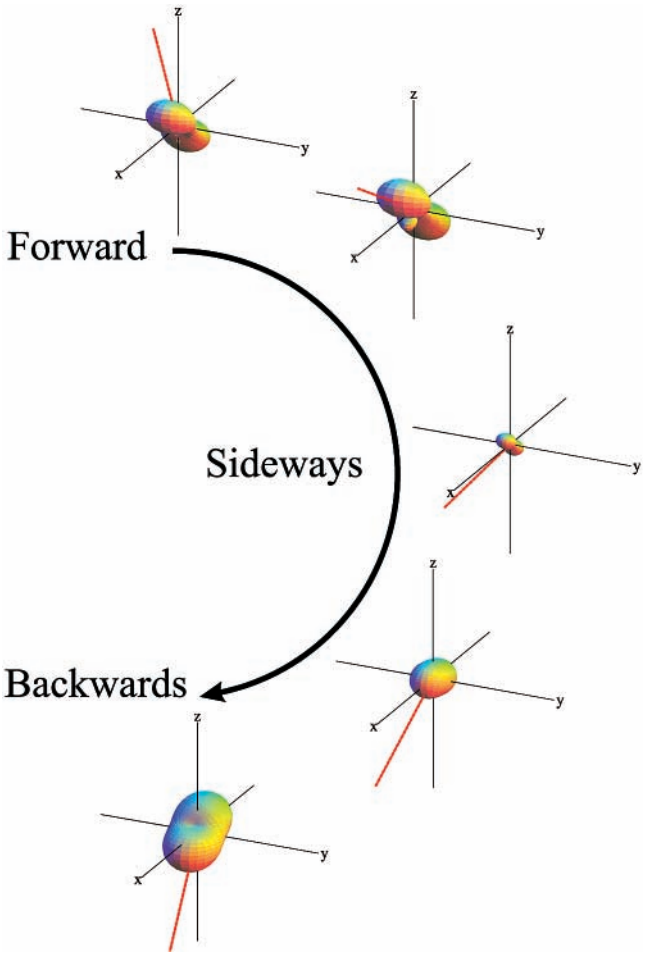

Figure 10. "Animations" of the polar plots representing the scattering angle dependence of the angular momentum polarization (see eq 4). The scattering angle is represented as the angle between the solid line and the *z* axis and defines the *zx* scattering plane.[23] Data are shown at representative scattering angles for the OH(Π(A″)) levels of OH($^2\Pi_{3/2}$, $v' = 0$, $N' = 5$). The behavior is typical of that found for the other OH(Π(A″)) levels probed and indicates the operation of torsional torques as the HNNO complex dissociates.[40]

are shown in Figure 10.[40] Here we have used eq 4 to reconstruct the rotational polarization distribution (in this case using only even moments with $k = 0$ and 2), which we have then represented in the form of a polar plot. The length of a vector drawn from the origin to the surface of the "lobe" represents the probability that $\mathbf{j}'$ lies in that direction. The red vector identifies the direction of OH recoil in the CM frame **w**, whereas the volume of the lobe is proportional to the differential cross-section weighted by a sin θ_t volume element (the CM *zx* plane is the scattering plane). For the channel shown, OH($v' = 0$, $N' = 5$), the scattering is principally in the forward and backward direction (see Figure 5). Note that because $\mathbf{j}'$ is aligned preferentially parallel to **w**, the motion of the OH is like that of a propeller. Such motion suggests that out-of-plane torsional forces play an important role as the HNNO complex rearranges and dissociates to OH + N_2 products.

Given our previous discussion of the similarities between the H + N_2O reaction and the photodissociation of $HN_3(\tilde{A})$, it should come as no surprise that in the latter system the NH($^1\Delta$) photofragments are formed highly rotationally aligned with $\mathbf{j}'||\mathbf{v}$,[82] consistent with the operation of strong torsional torques in the exit channel.[82,88] Interestingly, the strongest torsional-type alignment is observed in the HN($^1\Delta$) A' Λ-doublet level,[82] as opposed to the OH A'' level in the case of the H + N_2O reaction:[40] the different behavior probably reflects the different electronic symmetries of $HN_3(\tilde{A}^1A'')$ and $HNNO(\tilde{X}^2A')$.

6. Angular Momentum Orientation

Determining rotational angular momentum orientation, both in bimolecular reactions and in molecular photodissociation, is in its infancy compared with alignment measurements.[36,92,93] The observation of rotationally oriented NO produced from the 355 nm photolysis of NO_2 using *linearly* polarized light[94] is one of the few examples in which *molecular* rotational orientation has been detected[94−96] (see section 6.1.). However, it is only by determining orientation moments that a more complete reconstruction of the rotational polarization distribution (eq 4) can be made.

Product rotational orientation has been predicted for a number of bimolecular reactions.[23,39,86,89−91] We illustrate such effects by reference to QCT calculations on the O(^{1}D) + H_2 reac-

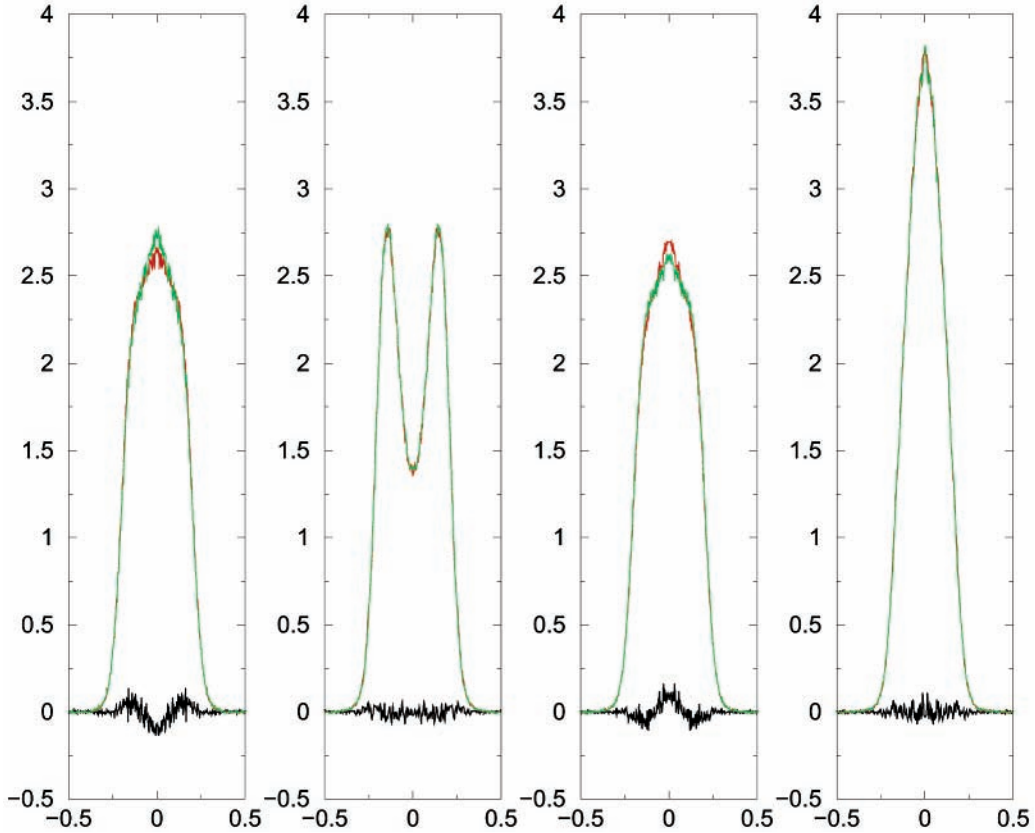

Figure 11. Raw experimental Doppler profiles for the NO ($v' = 0$, $N' = 29$) products of the 308 nm photodissociation of NO_2. The red and green data are the signals obtained with left and right circularly polarized probe light, whereas the black lines are the difference signals which depend solely on angular momentum orientation. The four panels show the signals obtained by varying the angle between the electric vector of the photolysis radiation and probe laser propagation vector: in the first and third panels from the left, the angle is ±45°, whereas in the second and forth panels, the angle is 0° and 90°. Note that in the latter two geometries the orientation signal must be zero.[96]

tion,[86,90] the rotational alignment for which has already been discussed. As noted in section 5, reaction on the ground state PES generates only modest angular momentum polarization.[86] In contrast to this behavior, reaction over the first excited $^1A''$ PES shows strong alignment (see section 5) *and* orientation. QCT calculated polar plots of the OH($v' = 4$, $j' = 2$) angular momentum polarization generated on the two PESs have been shown already in Figure 8.[86] In the case of reaction over the excited-state surface, note the strong orientation of $\mathbf{j}'$ along the $-y$ direction. For reasons of symmetry, orientation can only be observed perpendicular to the *zx* scattering plane: the polarization is an example of planar, or false, chirality, discussed recently by Cline and co-workers in the context of molecular photodissociation.[97] The mechanism responsible for the orientation generated on the $^1A''$ PES of the $O(^1D) + H_2$ reaction is believed to be the same as that observed in QCT calculations for the $F + H_2$ reaction and has been termed a repulsive abstraction mechanism.[89] Lower OH (and HF) vibrational states show the reverse orientation (i.e., the orientation is preferentially along the $+y$ axis), reflecting a qualitatively different reaction mechanism, termed repulsive insertion.[86,89]

6.1. $NO_2 + h\nu \rightarrow NO + O(^3P)$. We have used circularly polarized probe light to construct a pump−probe geometry which is sensitive to the odd moments of the angular momentum distribution.[36,96] Doppler-resolved LIF profiles recorded in such a geometry are shown in Figure 11, where the red and green profiles in each panel correspond to profiles recorded using right and left circularly polarized probe light, respectively, and the black profiles are the difference signals. The data were obtained for the NO($v' = 0$, $N' = 29$) photofragments generated following linearly polarized photolysis of NO_2 at 308 nm. To demonstrate that the difference signal is a genuine orientation effect, we determined how the orientation signal varies on rotation of the electric field vector of the photolysis light, ϵ, by increments of 45°. The difference signals shown in the first and third panels of Figure 11 are sensitive to orientation, but with opposite signs, whereas those in the second and fourth panels are known not to be sensitive to orientation and hence display a zero orientation signal.[36,96]

Doppler profiles were also recorded in a further eight geometries sensitive only to alignment and two geometries sensitive to both alignment and higher order orientation moments. The analysis of the full data set yielded the moments of the angular momentum distribution up to and including rank $k = 3$. Polar plots representing the polarization distribution as a function of NO recoil direction are shown in Figure 12. These plots are similar to those shown in Figure 10, but in this case, the *z* axis coincides with the transition dipole moment for the electronic transition involved in the photolysis step ($^2B_2 \leftarrow {}^2A_1$), which lies along the axis joining the two terminal oxygen atoms. As in Figure 10, the red vector represents the recoil velocity vector of the NO photofragment, $\mathbf{v}'$, and the distance from the origin to the surface of the lobe represents the probability of $\mathbf{j}'$ pointing in that direction. Note that, unlike the data shown in Figure 10, the polar plots shown in Figure 12, which now contain both even and odd *k* moments, are not symmetric about the *zx* plane.

The sense of rotation implied by the data shown in Figure 12 agrees with that predicted by a simple impulsive model in which a torque is applied to the nitrogen end of the departing NO moiety because of the energy released from the breaking bond (the orientation is also in the same sense as that determined

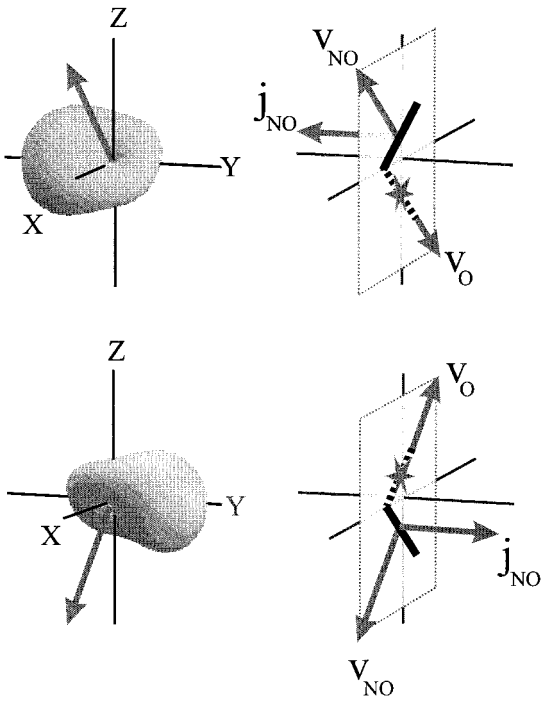

Figure 12. Distribution $P(\cos\theta_t,\omega_{j'})$ for the NO($v' = 0$, $N' = 29$) products of the 308 nm photodissociation of NO_2. The polar plots (left panels) show the semiclassical angular distribution of $\mathbf{j}'$ at two recoil angles θ_t (represented by the bold arrow in the left panels). The mutual orientation of the vectors is illustrated schematically in the panels on the right. Adapted from ref 96.

previously by Cline and co-workers at 355 nm[94]). Hence, the NO fragments recoiling in the positive *z* direction have their $\mathbf{j}'$ vectors pointing along the positive *y* direction, whereas those recoiling in the negative *z* direction have an opposite sense of rotation. However, more recent experiments in our group,[98] in which we have measured the angular distributions of the NO-($v' = 1$) $N' = 9$, 16, and 21 fragments, reveal that a simple trend of increasing orientation with N' is not adhered to. Unlike the rotational alignment, which *does* increase monotonically with N', the lowest order orientation moment only takes a significant nonzero value for the $N' = 16$ fragments, suggesting that more subtle dynamical processes influence the magnitude of the orientation than simple impulsive forces alone. In particular, the balance between bond angle opening and closing (bending) motions of the dissociating NO_2 species as it passes through the conical intersection between the $\tilde{B}$ and $\tilde{X}$ states is likely to play an important role in determining the NO rotational orientation.[99] Studies are currently in progress to exploit the same pump−probe methods to determine orientational effects in bimolecular reactions (see, for example, refs 23 and 100).

7. Conclusions and Forward Look

We hope to have shown how bulb measurements using the photon-initiated technique can be valuable in helping to elucidate the state-resolved dynamics of elementary bimolecular reactions, especially when supported by the results from high quality ab initio theory. However, there is always a need for the higher angular and energy resolution potentially achievable using skimmed molecular beams. One approach, which employs a similar strategy to that described here,[25] is to couple photon-initiation with REMPI, core extraction detection.[16] This technique has been exploited to great effect in recent years by Zare and co-workers.[16]

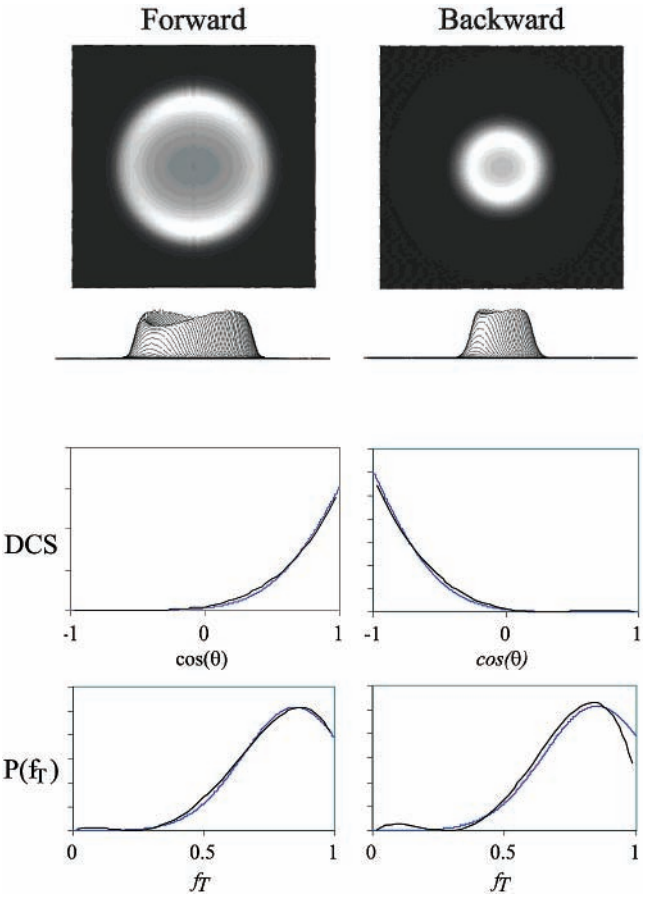

Figure 13. Upper panels: Simulated *raw ion images* for the CH_3 products of the $O(^1D) + CH_4 \rightarrow OH + CH_3$ reaction, assuming $O(^1D)$ atom production via photodissociation of N_2O. The simulations assume the CM angular and kinetic energy release distributions shown in the lower panels (black lines). Also shown as blue lines in the lower panels are the returned CM distributions obtained by least-squares fitting the two nonzero moments of these images.

An alternative scheme is to couple photon-initiation with REMPI velocity map[101] ion imaging detection.[102,103] The viability of this approach has recently been demonstrated by Kitsopoulos and co-workers in a study of the $Cl + C_2H_6$ reaction.[104] We illustrate the potential of the technique by reference to the $O(^1D) + CH_4 \rightarrow OH + CH_3$ reaction.[105] In the upper panel of Figure 13, we show simulated raw ion images assuming different forms for the CM angular scattering, and kinetic energy release distributions are displayed in lower panels of the same figure. The latter, in addition, show the CM distributions returned from fits to the simulated images. The least-squares fitting has been performed very efficiently by using the two (radially dependent) nonzero moments of the raw images shown in the upper panel of Figure 13. As can be seen, the CM distributions of interest are returned very reliably with this procedure. More importantly, it is anticipated that the angular and energy resolution of the technique will typically be about an order of magnitude greater than for the bulb experiments described in this paper.

Acknowledgment. First we thank present and past members of, and visitors to, the group, who have contributed to the work described, in particular, Mark Bass, Professor Itamar Burak, Dr. Simon D. Gatenby, Dr. D. Melissa Joseph, Dr. Gavin Markillie, and Denys Minayev. It is a pleasure to thank Professor Javier Aoiz and his group, at the Complutense University, Madrid, with whom we have enjoyed a productive collaboration for

many years, and my colleagues at Oxford University, Professor John P. Simons and Dr. David E. Manolopoulos, for their support and numerous helpful discussions. We are also very grateful to the EPSRC, The Royal Society, and the EU (through Project No. HPRN-CT-1999-00007) for their generous financial support.

References and Notes

(1) Levine, R. D.; Berstein, R. B. *Molecular Reaction Dynamics and Chemical Reactivity*; Oxford University Press, Inc.: New York, 1987.
(2) See for example Clary, D. C. *Phys. Chem. Chem. Phys.* **1999**, *1*, 1173.
(3) Miller, W. H. *Acc. Chem. Res.* **1993**, *26*, 174.
(4) Bowman, J. M.; Schatz, G. C. *Annu. Rev. Phys. Chem.* **1995**, *46*, 169.
(5) See, for example: Aoiz, F. J.; Banares, L.; Herrero, V. J. *J. Chem. Soc., Faraday. Trans.* **1998**, *94*, 2483.
(6) Honvault, P.; Launay, J.-M. *J. Chem. Phys.* **2001**, *114*, 1057.
(7) Zhang, D. H.; Collins, M. A.; Lee, S.-Y. *Science* **2000**, *290*, 961.
(8) Clary, D. C. *Science* **1998**, *279*, 1879.
(9) See, for example: Yang, M.; Zhang, D. H.; Collins, M. A.; Lee, S.-Y. *J. Chem. Phys.* **2001**, *114*, 4759.
(10) Alexander, M. H.; Manolopoulos, D. E.; Werner, H.-J. *J. Chem. Phys.* **2000**, *113*, 11084.
(11) Yarkony, D. R. *J. Phys. Chem.* **2001**, *105*, 6277.
(12) Ho, T.-S.; Hollebeek, T.; Rabitz, H.; Harding, L. B.; Schatz, G. C. *J. Chem. Phys.* **1996**, *105*, 10472. Schatz, G. C.; Papaioannou, A.; Pederson, L. A.; Harding, L. B.; Hollebeek, T.; Ho, T. S.; Rabitz, H. *J. Chem. Phys.* **1997**, *107*, 2340. Schatz, G. C.; Pederson, L. A.; Kuntz, P. J. *Faraday Discuss. Chem. Soc.* **1997**, *108* 357.
(13) Schnieder, L.; Seekamp-Rahn, K.; Wrede, E.; Welge, K. H. *J. Chem. Phys.* **1997**, *107*, 6175, and references therein.
(14) Manolopoulos, D. E. *J. Chem. Soc., Faraday Trans.* **1997**, *93*, 673. Skodje, R. T.; Skouteris, D.; Manolopoulos, D. E.; Lee, S.-H.; Dong, F.; Liu, K. *Phys. Rev. Lett.* **2000**, *85*, 1206, and references therein.
(15) Orr-Ewing, A. J.; Zare, R. N. *Annu. Rev. Phys. Chem.* **1994**, *45*, 315.
(16) Orr-Ewing, A. J.; Zare, R. N. In *Chemical dynamics and kinetics of small free radicals*; Liu, K., Wagner, A. L., Eds.; World Scientific: Singapore, 1995; Part II, p 936.
(17) Orr-Ewing, A. J. *J. Chem. Soc., Faraday Trans.* **1996**, *92*, 881.
(18) Brouard, M.; Simons, J. P. In *Chemical dynamics and kinetics of small free radicals*; Liu, K., Wagner, A. L., Eds.; World Scientific: Singapore, 1995; Part II, p 936. Alexander, A. J.; Brouard, M.; Kalogerakis, K. S.; Simons, J. P. *Chem. Soc. Rev.* **1998**, *27*, 405.
(19) Simons, J. P. *J. Chem. Soc., Faraday. Trans.* **1997**, *93*, 4095. Simons, J. P. *Faraday Discuss.* **1999**, *113*, 1.
(20) Valentini, J. J. *Annu. Rev. Phys. Chem.* **2001**, *52*, 15.
(21) Norrish, R. G. W.; Porter, G. *Proc. R. Soc. London* **1952**, *A210*, 439.
(22) Aoiz, F. J.; Brouard, M.; Enriquez, P. A.; Sayos, R. *J. Chem. Soc., Faraday Trans.* **1993**, *89*, 1427.
(23) Aoiz, F. J.; Brouard, M.; Enriquez, P. A. *J. Chem. Phys.* **1996**, *105*, 4981.
(24) Shafer, N. E.; Orr-Ewing, A. J.; Simpson, W. R.; Xu, H.; Zare, R. N. *Chem. Phys. Lett.* **1993**, *212*, 155. Simpson, W. R.; Orr. Ewing, A. J.; Zare, R. N. *Chem. Phys. Lett.* **1993**, *212*, 163.
(25) Shafer-Ray, N. E.; Orr-Ewing, A. J.; Zare, R. N. *J. Phys. Chem.* **1995**, *99*, 7591.
(26) Wolfrum, J. In *Selectivity in Chemical Reactions*; Whitehead, C. J., Ed.; Nato ASI Series; Kluwer Academic Publishers: Norwell, MA, 1988; Vol. 245, p 23. A summary of recent results on the $H + H_2O$ reaction can be found in Szichman, H.; Baer, M.; Volpp, H. R.; Wolfrum, J. *J. Chem. Phys.* **1999**, *111*, 567.
(27) Houston, P. L. *J. Phys. Chem.* **1987**, *91*, 5388. Simons, J. P. *J. Phys. Chem.* **1987**, *91*, 5378.
(28) Zare, R. N.; Herschbach, D. R. *Proc. IEEE* **1963**, *51*, 173.
(29) Brouard, M.; Burak, I.; Gatenby, S. D.; Markillie, G. A. J. *Chem. Phys. Lett.* **1998**, *287*, 682.
(30) Kim, H. L.; Wickramaaratchi, M. A.; Zheng, X.; Hall, G. E. *J. Chem. Phys.* **1994**, *101*, 2033. Fei, R.; Zheng, X. S.; Hall, G. E. *J. Phys. Chem. A* **1997**, *101*, 2541.
(31) Brouard, M.; Burak, I.; Markillie, G. A. J.; McGrath, K.; Vallance, C. *Chem. Phys. Lett.* **1997**, *281*, 97.
(32) Brouard, M.; Duxon, S. P.; Enriquez, P. A.; Simons, J. P. *J. Chem. Phys.* **1992**, *97*, 7414.
(33) Gilbert, F. P.; Maitland, G.; Watson, A.; McKendrick, K. G. *J. Chem. Soc., Faraday Trans.* **1993**, *89*, 1527.
(34) Green, F.; Hancock, G.; Orr-Ewing, A. J. *Faraday Discuss. Chem. Soc.* **1991**, *91*, 79. Green, F.; Hancock, G.; Orr-Ewing, A. J.; Brouard, M.; Duxon, S. P.; Enriquez, P. A.; Sayos, R.; Simons, J. P. *Chem. Phys. Lett.* **1991**, *182*, 568.
(35) Greene, C. H.; Zare, R. N. *J. Chem. Phys.* **1983**, *78*, 6742.
(36) Kummel, A. C.; Sitz, G. O.; Zare, R. N. *J. Chem. Phys.* **1988**, *88*, 7357.
(37) Dixon, R. N. *J. Chem. Phys.* **1986**, *85*, 1866.
(38) de Miranda, M. P.; Clary, D. C. *J. Chem. Phys.* **1997**, *106*, 4509.
(39) de Miranda, M. P.; Aoiz, F. J.; Bañares, L.; Sáez Rábanos, V. *J. Chem. Phys.* **1999**, *111*, 5368.
(40) Brouard, M.; Gatenby, S. D.; Joseph, D. M.; Vallance, C. *J. Chem. Phys.* **2000**, *113*, 3162.
(41) Jacobs, A.; Volpp, H.-R.; Wolfrum, J. *Chem. Phys. Lett.* **1994**, *218*, 51; *J. Chem. Phys.* **1994**, *100*, 1936. Jacobs, A.; Volpp, H.-R.; Wolfrum, J. *Chem. Phys. Lett.* **1992**, *196*, 249. Koppe, S.; Laurent, T.; Naik, P. D.; Volpp, H.-R.; Wolfrum, J. *Can. J. Chem.* **1994**, *72*, 615.
(42) Castillo, J. F.; Santamaria, J. *J. Phys. Chem. A* **2000**, *104*, 10414.
(43) Castillo, J. F.; Aoiz, F. J.; Banares, L.; Santamaria, *J. Chem. Phys. Lett.* **2000**, *329*, 517.
(44) Bradley, K. S.; Schatz, G. C. *J. Chem. Phys.* **1998**, *108*, 7994.
(45) Troya, D.; Gonzalez, M.; Schatz, G. C. *J. Chem. Phys.* **2001**, *114*, 8397. Troya, D.; Lendvay, G.; Gonzalez, M.; Schatz, G. C. *Chem. Phys. Lett.* **2001**, *343*, 420.
(46) Schatz, G. C.; Elgersma, H. *Chem. Phys. Lett.* **1980**, *73*, 21.
(47) Ochoa de Aspuru, G.; Clary, D. C. *J. Phys. Chem.* **1998**, *102*, 9631.
(48) Wu, G.; Schatz, G. C.; Lendvay, G.; Fang, D.-C.; Harding, L. B. *J. Chem. Phys.* **2000**, *113*, 3150, 7712.
(49) Sinha, A.; Hsiao, M. C.; Crim, F. F. *J. Phys. Chem.* **1991**, *95*, 8263. Metz, R. B.; Thoemke, J. D.; Pfeiffer, J. M.; Crim, F. F. *J. Chem. Phys.* **1993**, *99*, 1744.
(50) Alexander, M. H., et al. *J. Chem. Phys.* **1988**, *89*, 1749.
(51) Balint-Kurti, G. G. *J. Chem. Phys.* **1986**, *84*, 4443.
(52) Hausler, D.; Andresen, P.; Schinke, R. *J. Chem. Phys.* **1987**, *87*, 3949.
(53) Clary, D. C. *J. Chem. Phys.* **1991**, *95*, 7298; **1992**, *96*, 3656. Nyman, G.; Clary, D. C. *J. Chem. Phys.* **1993**, *99*, 7774.
(54) Clary, D. C. *J. Phys. Chem.* **1995**, *99*, 13664.
(55) Brouard, M.; Gatenby, S. D.; Joseph, D. M.; Markillie, G. A. J.; Minayev, D.; O'Keeffe, P.; Vallance, C. *J. Chem. Phys.* **2001**, *114*, 6690.
(56) Brouard, M.; Minayev, D.; O'Keeffe, P. Manuscript in preparation.
(57) Aoiz, F. J.; Castillo, J. F. Personal communication.
(58) Drukker, K.; Schatz, G. C. *J. Chem. Phys.* **1999**, *111*, 2451. Gray, S. K.; Petrongolo, C.; Drukker, K.; Schatz, G. C. *J. Phys. Chem. A* **1999**, *103*, 9448.
(59) Rackham, E. J.; Huarte-Larranaga, F.; Manolopoulos, D. E. *Chem. Phys. Lett.* **2001**, *343*, 356.
(60) Aoiz, F. J.; Bañares, L.; Herrero, V. J. *Chem. Phys. Lett.* **1999**, *310*, 277.
(61) Dobbyn, A. J.; Knowles, P. K. *Mol. Phys.* **1997**, *91*, 1107; *Faraday Discuss.* **1998**, *110*, 247.
(62) Aoiz, F. J.; Banares, L.; Brouard, M.; Castillo, F. J.; Herrero, V. J. *J. Chem. Phys.* **2000**, *113*, 5339.
(63) Alagia, M.; Balucani, N.; Cartechini, L.; Casavecchia, P.; van Kleef, E. H.; Volpi, G. G.; Kuntz, P. J.; Sloan, J. J. *J. Chem. Phys.* **1998**, *108*, 6698.
(64) Hsu, Y.-T.; Liu, K.; Pederson, L. A.; Schatz, G. C. *J. Chem. Phys.* **1999**, *111*, 7921. Hsu, Y.-T.; Liu, K.; Pederson, L.A.; Schatz, G. C. *J. Chem. Phys.* **1999**, *111*, 7931. Lee, S.-H.; Liu, K. *J. Chem. Phys.* **1999**, *111*, 4351.
(65) Aoiz, F. J.; Banares, L.; Castillo, J. F.; Brouard, M.; Denzer, W.; Vallance, C.; Honvault, P.; Launay, J.-M.; Dobbyn, A. J.; Knowles, P. J. *Phys. Rev. Lett.* **2001**, *86*, 1729.
(66) Liu, X.; Lin, J. J.; Harich, S.; Schatz, G. C.; Yang, X. *Science* **2000**, *289*, 1536; *J. Chem. Phys.* **2000**, *113*, 1325; *Phys. Rev. Lett.* **2001**, *86*, 408. Gray, S. K.; Balint-Kurti, G. G.; Schatz, G. C.; Lin, J. J.; Liu, X.; Harich, S.; Yang, X. *J. Chem. Phys.* **2000**, *113*, 7330.
(67) Aoiz, F. J.; Banares, L.; Castillo, J. F. Personal communication.
(68) Alagia, M.; Balucani, N.; Casavecchia, P.; Stranges, D.; Volpi, G. G. *J. Chem. Phys.* **1993**, *98*, 2459. Alagia, M.; Balucani, N.; Casavecchia, P.; Stranges, D.; Volpi, G. G.; Clary, D. C.; Kliesch, A.; Werner, H.-J. *Chem. Phys.* **1996**, *207*, 389.
(69) Strazisar, B. R.; Lin, C.; Davis, H. F. *Science* **2000**, *290*, 958.
(70) Adelman, D. E.; Filseth, S. V.; Zare, R. N. *J. Chem. Phys.* **1993**, *98*, 4636. Bronikowski, M. J.; Simpson, W. R.; Zare, R. N. *J. Phys. Chem.* **1993**, *97*, 2194.
(71) Hawthorne, G.; Sharkey, P.; Smith, I. W. M. *J. Chem. Phys.* **1998**, *108*, 4693. Barnes, P. W.; Sharkey, P.; Sims, I. R.; Smith, I. W. M. *Faraday Discuss.* **1999**, *113*, 167. Barnes, P. W.; Sims, I. R.; Smith, I. W. M.; Lendvay, G.; Schatz, G. C. *J. Chem. Phys.* **2001**, *115*, 4586.
(72) Aoiz, F. J.; Bañares, L.; Herrero, V. J.; Sáez Rábanos, V.; Tanarro, I. *J. Phys. Chem.* **1997**, *101*, 6156.
(73) Zhang, D. H.; Light, J. C. *J. Chem. Phys.* **1996**, *105*, 1291.
(74) Brouard, M.; Burak, I.; Gatenby, S. D.; Hart, D.; Minayev, D. *J. Chem. Phys.* **1999**, *110*, 11335.

(75) Brouard, M.; Burak, I.; Gatenby, S. D. *Phys. Chem. Chem. Phys.* **2000**, *2*, 715.
(76) Bradley, K. S.; McCabe, P.; Schatz, G. C.; Walch, S. P. *J. Phys. Chem.* **1995**, *102*, 6696. Bradley, K. S.; Schatz, G. C. *J. Chem. Phys.* **1997**, *106*, 8464.
(77) Walch, S. P. *J. Chem. Phys.* **1993**, *98*, 1170.
(78) Brouard, M.; Lambert, H. M.; Rayner, S. P.; Simons, J. P. *Mol. Phys.* **1996**, *89*, 403; Brouard, M.; Hughes, D. W.; Kalogerakis, K. S.; Simons, J. P. *J. Phys. Chem.* **1998**, *102*, 9559.
(79) Brouard, M.; Hughes, D. W.; Kalogerakis, K. S.; Simons, J. P. *J. Chem. Phys.* **2000**, *112*, 4557.
(80) Hoffmann, G.; Oh, D.; Iams, H.; Wittig, C. *Chem. Phys. Lett.* **1989**, *155*, 356. Hoffmann, G.; Oh, D.; Wittig, C. *J. Chem. Soc., Faraday Trans. 2* **1989**, *85*, 1141.
(81) Hanisco, T. F.; Kummel, A. C. *J. Phys. Chem.* **1993**, *97*, 7242.
(82) Gericke, K.-H.; Theinl, R.; Comes, F. J. *J. Chem. Phys.* **1990**, *92*, 6548. Gericke, K.-H.; Haas, T.; Lock, M.; Theinl, R.; Comes, F. J. *J. Phys. Chem.* **1991**, *95*, 6104. Gericke, K.-H.; Lock, M.; Fasold, R.; Comes, F. J. *J. Chem. Phys.* **1992**, *96*, 422.
(83) Herschbach, D. R. *Faraday Discuss. Chem. Soc.* **1973**, *55*, 233.
(84) Chu, J.-J.; Marcus, P.; Dagdigian, P. J. *J. Chem. Phys.* **1990**, *93*, 257.
(85) Case, D. E.; Herschbach, D. R. *Mol. Phys.* **1975**, *30*, 1537. Case, D. E.; McClelland, G. M.; Herschbach, D. R. *Mol. Phys.* **1978**, *35*, 541.
(86) Alexander, A. J.; Aoiz, F. J.; Banares, L.; Brouard, M.; Simons, J. P. *Phys. Chem. Chem. Phys.* **2000**, *2*, 571.
(87) Brouard, M.; Burak, I.; Hughes, D. W.; Kalogerakis, K. S.; Simons, J. P. *J. Chem. Phys.* **2000**, *113*, 3172.
(88) Meier, U.; Staemmler, V. *J. Phys. Chem.* **1991**, *95*, 6111.
(89) Aoiz, F. J.; Brouard, M.; Herrero, V. J.; Saez Rabanos, V.; Stark, K. *Chem. Phys. Lett.* **1997**, *264*, 487.
(90) Aoiz, F. J.; Banares, L.; Castillo, J. F.; Martinez-Haya, B.; de Miranda, M. P. *J. Chem. Phys.* **2001**, *114*, 8328.
(91) Wang, M.-L.; Han, K.-l.; He, G.-Z. *J. Phys. Chem. A* **1998**, *102*, 10204.
(92) Rakitzis, T. P.; Kandel, S. A.; Alexander, A. J.; Kim, Z. H.; Zare, R. N. *Science* **1998**, *281*, 1346; *J. Chem. Phys.* **1999**, *110*, 3351. Kim, Z. H.; Alexander, A. J.; Kandel, S. A.; Rakitzis, T. P.; Zare, R. N. *Faraday Discuss. Chem. Soc.* **1999**, *113*, 27.
(93) Rakitzis, T. P.; Samartzis, P. C.; Kitsopoulos, T. N. *J. Chem. Phys.* **1999**, *111*, 10415.
(94) Nestorov, V. K.; Cline, J. I. *J. Chem. Phys.* **1999**, *111*, 5287.
(95) Hasselbrink, E.; Waldeck, J. R.; Zare, R. N. *Chem. Phys.* **1988**, *126*, 191. Black, J. F.; Hasselbrink, E.; Waldeck, J. R.; Zare, R. N. *Mol. Phys.* **1990**, *71*, 1143.
(96) Brouard, M.; Joseph, D. M.; Minayev, D.; O'Keeffe, P. *Phys. Rev. Lett.* **2001**, *86*, 2249.
(97) Uberna, R.; Hinchliffe, R. D.; Cline, J. I. *J. Chem. Phys.* **1995**, *103*, 1934.
(98) Brouard, M.; Ingham, D.; O'Keeffe, P. Manuscript in preparation.
(99) Katagiri, H.; Kato, S. *J. Chem. Phys.* **1993**, *99*, 8805.
(100) Rakitzis, T. P.; Kandel, S. A.; Zare, R. N. *J. Chem. Phys.* **1997**, *107*, 9382. Rakitzis, T. P.; Kandel, S. A.; Lev-On, T.; Zare, R. N. *J. Chem. Phys.* **1997**, *107*, 9392.
(101) Eppink, A. T. J. B.; Parker, D. H. *Rev. Sci. Instrum.* **1997**, *68*, 3477.
(102) Heck, A. J. R.; Chandler, D. W. *Annu. Rev. Phys. Chem.* **1995**, *46*, 335.
(103) Houston, P. L. *J. Phys. Chem.* **1996**, *100*, 12757.
(104) Samartzis, P. C.; Smith, D. J.; Rakitzis,; Kitsopoulos, T. N. *Chem. Phys. Lett.* **2000**, *324*, 337.
(105) Bass, M. J.; Brouard, M.; Vallance, C. Manuscript in preparation.